Published on Nucl. Instru. and Meth. A 363 (1995) 538.

A study of the charge cluster characteristics and spatial resolution of a silicon microstrip detector

Yuan-Hann Chang, Augustine E. Chen, Suen R. Hou[1], Willis T. Lin
Physics Department, National Central University,
Chungli, Taiwan, R.O.C

Abstract

The analysis on test beam data of a large silicon microstrip detector is presented. The spatial resolution has been studied with full GEANT simulation to calculate the systematic uncertainty due to multiple scattering. Several cluster position-finding algorithms have been applied for inclined tracks. The cluster profile and spatial resolution have the predicted geometrical correlation to the track angle.

[1]Corresponding auther, Tel +41 22 767 9358, Fax +41 22 782 2601, e-mail suenhou@vxcern.cern.ch.

1 Introduction

The success of silicon detector in high energy experiments leads to growing interest in large silicon tracking devices. Here we present the analysis of test beam data on a silicon microstrip detector of large active area. We first outline the parameters of test devices and the test beam setup. The passage of a particle track in the detector is seen as a charge cluster of adjacent strips. The data processing and cluster-finding algorithm rely on clean subtraction of pedestal and common mode shift of each readout channel. The η distribution characterizes the non-linear charge sharing between strips. With the η correction, the spatial resolution has been extensively studied by linear track fitting with the multiple scattering calculated by full GEANT [1] simulation and the intrinsic resolution embedded as a Gaussian smearing. For tracks with non-zero inclined angles to the detector plane, the cluster profile has an angular dependence according to the geometrical scaling factor, and shows no effect to the charge collection efficiency. The impact position of inclined tracks has been studied using different cluster position-finding algorithms. The angular dependence of the position resolution will also be discussed.

2 Test devices and test beam Setup

The devices tested include two AC-coupled silicon microstrip detectors ($N5, N9$) of large active area of 40×80 mm^2. These detectors are single-sided with strip pitch of 25 μm and readout pitch of 50 μm. The microstrips are manufacture on 4kΩ-cm n-type wafer with thickness of 320 μm. The coupling capacitor is formed by multilayer dielectric called ONO. It consists of an 100 nm oxide layer, and a 200 nm nitride layer which gives a capacitance equivalent to a 200 nm oxide layer. A second oxidation layer is used to anneal the interface between the oxide and nitride layers. The ONO structure is highly pinhole-free and has good characteristics for breakdown voltage and moisture protection. The total leakage current measured is about 4 μA. Detail description can be found in ref. [2].

The test beam was performed at the X3 complex of CERN-SPS with 50 GeV electron beam. In the first setup in fig. 1, the test devices ($N5, N9$) were aligned with six reference detectors ($J1, J2, N3, N4, C1, C2$) for the study of spatial resolution. For the angular dependence of inclined tracks, the second setup has test devices assembled for two-dimensional measurement with three sets of reference detectors in the beam line.

For each detector, the charge collected by each strip is amplified and multiplexed by the SVX chip [3]. The amplified analog signals are then digitized with 8 bits dynamic range by an SRS-SDA CAMAC system [4]. The CAMAC system is interfaced by GPIB to a PC for data acquisition.

3 Data processing and cluster-finding algorithm

During the data taking, calibration events were randomly triggered between spills of beam particles. These events are used to determine the pedestal and noise level. For each event, the common mode base-line shift (C) is calculated as the average of raw ADC value (A_i^{raw}) over the total of 128 channels of one SVX. The pedestal of each channel (dP_i) is then calculated as the mean of ($A_i^{raw} - C$) of all calibration events. The noise level (σ_{Ni}) is the standard deviation of the distribution of dP_i. The values of σ_{Ni} of the same SVX are rather uniform, the average

(σ_N) is used in the analysis.

For event triggered by the beam particle, the common shift is first calculated and the signal (Q_i) of each channel is obtained as the net ADC after subtraction of the pedestal and the common mode shift, namely, $Q_i = A_i^{raw} - dP_i - C$.

Along the particle track in the detector, the charge generated by ionization mechanism is collected by one or more adjacent strips. A particle passage is therefore represented by the cluster of these adjacent channels. In this analysis, the cluster is determined by the following requirements to separate from random noise.

1) *Locating the channel of local maximum signal Q_i above a threshold of $3\sigma_N$;*

2) *Stepping up and down the neighboring strips till Q_i is below $1\sigma_N$;*

3) *Summing up Q_i of selected strips, and requiring it be larger than $6\sigma_N$.*

The distribution of cluster total charge (fig. 2) is fitted to a Gaussian convoluted Landau distribution. The signal to noise ratio is taken as the ratio of the most probable value of Landau distribution to σ_N of pedestal distribution. Signal to noise ratio of about 23 was obtained for the detectors tested by normally incident tracks.

To locate the particle impact position, the cluster position in units of readout pitch is first calculated by center-of-gravity (X_{COG}) weighted by strip signal, with angular correction for alignments. The charge sharing between strips is not linear and therefore a η correction to X_{COG} is applied [5]. The variable η for clusters of more than one strip is defined as

$$\eta = \frac{Q_r}{Q_r + Q_l}$$

where Q_r (Q_l) are the charge sum of strips to the right (left) of X_{COG}. The η distribution, $f(\eta)$, of the $N9$ detector is shown in fig. 3.

The beam particles are triggered with a beam spot much large than the readout pitch and therefore the impact points are believed to be uniformly distributed between two neighboring strips. With the assumption that the charge sharing between the two neighboring strips is independent of the total charge, the η distribution correlates the charge sharing between channels and the impact coordinate of the particle. The absolute coordinate of the cluster position is corrected by the η value by:

$$X_\eta = \left(|X_{COG}| + \frac{\int_0^\eta f(\eta)}{\int_0^1 f(\eta)} \right) \times p$$

where p is the readout pitch and $|X_{COG}|$ is the coordinate of the strip to the direct left of X_{COG}. The $(X_\eta - X_{max})$ distribution of $N9$ is shown in fig. 4, where X_{max} is the position of the strip with maximum signal in the cluster.

In both distributions of η and $(X_\eta - X_{max})$, the components are classified into two-strip clusters (dash line) and clusters of more than two strips (dot line). The two-strip clusters favor to have η close to 0 and 1, that is, occur more often when the particle impact positions are close to readout strips. While the clusters of more than two strips are favored when the impact positions are in the middle between two readout strips. The detectors tested have intermediate strip between readout strips, which is characterized by the the bump at $\eta \sim 0.5$ in fig. 3. The presence of the middle bump helps to reduce the peak to valley ratio, which improves the spatial resolution that will be discussed in the next section. As the SVX chip has fixed cycle for the multiplexing of all channels, the tail part of signals are truncated which contribute to the asymmetry seen in the η distribution.

4 Spatial resolution and Monte Carlo simulation

The spatial resolution has been studied by unweighted linear least square fit on the particle track. The residual of the fit contains intrinsic resolution and systematic uncertainty from multiple Coulomb scattering. Practicing on the data of the first setup, that has total six detectors measuring the same coordinate, we have performed the fit with all six detectors as well as five detectors excluding alternatively each one. The rms of residuals obtained are listed in table 1.

In the unweighted fit, the residuals of the measurements depend not only on the intrinsic resolution, but also on the multiple scattering and the relative location of the detectors in the setup. We use a full GEANT simulation of the test beam setup to calculate the effect of multiple scattering by 50 GeV electrons with impinging angle distributed according to the data. The intrinsic resolution of each detector is implanted as a Gaussian smearing at the impact position. Assuming the intrinsic resolutions are the same for the various types of detectors used in the beam line, the rms of residuals of the unweighted linear fit on the simulation of all six detectors are plotted in fig. 5. In fig. 6 the rms of residuals of the detector excluded in the fit are shown. In comparison, the rms of residuals of data from the same fitting scheme are also plotted.

To reproduce the same residual as of the data, the rms of Gaussian smearing that simulates each individual detector resolution has been varied iteratively for the best agreement of both fitting schemes. The rms of residuals from MC simulation are also listed in table 1, with the corresponding rms of Gaussian smearing used. The intrinsic resolution thus obtained for the $N9$ detector is $3.5 \pm 1.0 \mu$m. The residual distribution of data(solid line) and MC(dot line) are shown in fig. 7, where a Gaussian fit is performed on data. A symmetrical distribution in data illustrates the achievement in the analysis on detector alignment, η correction on the cluster position, and the linear track fitting.

Concerning possible systematic uncertainty from the fitting program, a second fitting procedure has been practiced for comparison. We use the linear track fitting algorithm in ref. [6] which takes into account the kink angle of multiple scattering at each detector plane. The intrinsic resolution of all detectors obtained are compatible within 0.2 μm to the results of unweighted linear fit.

The detection efficiency has been evaluated while applying the linear fit with one detector excluded. To have the linear fit performed, detectors participated in the fit should have at least one cluster found. We search clusters on the detector excluded in the fit within a window of ± 500 μm from the predicted position by the fit. Regions masked dead for bad bonding and hot channels are excluded. The detection efficiency thus found is above $99.5 \pm 0.5\%$ for the test detectors and all reference detectors.

5 Cluster profile of inclined tracks

In practical application, particle impings the detector at arbitrary incidence angle. The second setup in fig. 1 can have the test devices rotated at chosen angle to study the effect of angular dependence. The four sets of detectors each has one (*horizontal*) detector measuring the horizontal coordinate, and one (*vertical*) detector measuring the vertical coordinate.

The projections of the particle track at angle θ are drawn in fig. 8 for test devices measuring horizontal and vertical coordinates respectively. The passage length increases as $1/\cos\theta$, which results in an $1/\cos\theta$ dependence of the total charge. The sagitta on *horizontal* detector, $W = L \times$

Data/MC	$N4$	$N9$	$J1$	$N3$	$C1$	$C2$
fit^{all}	4.4/4.3	4.1/4.1	8.4/8.6	5.6/5.7	6.7/6.6	7.3/7.6
fit^{ext}(C2)	3.8/3.9	3.9/4.0	7.7/7.9	5.4/5.0	5.9/5.3	12.7/12.6*
fit^{ext}(C1)	4.4/4.3	4.1/4.0	8.3/8.3	5.9/6.0	9.4/9.7*	6.5/6.5
fit^{ext}(N3)	4.3/4.2	4.0/4.1	8.6/8.6	7.4/7.3*	6.5/6.7	6.9/7.2
fit^{ext}(J1)	3.5/3.7	3.6/3.8	10.6/10.3*	6.0/6.1	6.0/6.6	7.0/7.1
fit^{ext}(N9)	3.9/3.7	7.1/7.1*	8.4/8.3	5.8/5.7	6.7/6.6	7.5/7.5
fit^{ext}(N4)	8.8/9.0*	4.1/3.9	7.9/7.8	5.8/5.7	6.5/6.5	7.1/7.3
$\sigma_{I.R.}$	5.8	3.5	8.7	5.1	6.8	10.6

Table 1: The rms of residuals of linear track fitting on data/MC; fit^{all} has all detectors included in the fit, fit^{ext} has one detector excluded in the fit as marked by (*). The bottom row ($\sigma_{I.R.}$) has the rms of Gaussian smearing that simulates the intrinsic resolution. The J and C detectors do not have intermediate strip, thus larger value of intrinsic resolution are expected.

$\tan\theta$, trespasses more strips that implies the number of strip per cluster increases proportional to $\tan\theta$.

The distribution of cluster total charge measured by the *vertical* detector for θ equal 0°, 15°, 30°, and 45° are shown in fig. 9. The most probable value of Landau distribution obtained as the function of θ is plotted in fig. 10 for both *horizontal* and *vertical* detectors. We found good agreement with the geometrical scaling of $Q \propto 1/\cos\theta$.

The width of cluster profile as the function of θ has been studied by the *horizontal* detector. Plotted in fig. 11 are the average charge collected by one strip at various θ angle versus the distance of the strip to the cluster center position. The calculation of cluster position will be discussed in the next section. From the corresponding distribution in fig. 11, the FWHM of the cluster profile are drawn in fig. 12 as the function of θ angle. The width increases in good agreement with the sagitta of W=320μm$\times\tan\theta$.

The cluster profiles seen in fig. 11 are symmetric to cluster position. As illustrated in fig. 8, the collection of charge from the track ionization by adjacent strips correspond to different depth of charge drifting. A symmetrical cluster profile indicates that the charge collection efficiency is independent of the location in depth of the ionization.

6 Spatial resolution of inclined tracks

The clusters of inclined tracks to the strip reading direction have cluster width much wider than those of perpendicular tracks. Therefore the η algorithm for determining the cluster position is not necessarily the most feasible method. The other two algorithms we have applied for finding the cluster position are [7]

1) *The central-of-gravity (COG) method* : the cluster position is determined by the constituent strips position (X_i) weighted by the strip signal (Q_i);

$$X_{COG} = \frac{\sum_i Q_i X_i}{\sum_i Q_i}$$

2) *The head-tail method* : for clusters of more than two strips, the position is determined by the edge two strip positions with correction on charge difference assuming the charge collected by the edge two strips are proportional to the path length covered, that is,

$$X = \frac{(X_{first} + X_{last})}{2} - (\frac{Q_{first}}{Q_{ave}} - \frac{Q_{last}}{Q_{ave}}) \times p$$

where Q_{ave} is the averaged charge per strip of the cluster and p is the readout pitch.

We found that for tracks of $\theta = 15°$, the COG method render the best resolution. As for tracks of $\theta = 30°$ and $45°$, the head-tail method gives the best results according to the residual of linear fit on tracks.

The intrinsic resolution of test detectors by inclined tracks has been studied by the unweighted linear track fitting in which the detectors are excluded in the fit. The residual width of the measurement is much larger than the width of multiple scattering. To calculate the intrinsic resolution, we apply quadrature subtraction of rms of the multiple scattering from the residual of linear track fitting. At θ equals $45°$, the intrinsic resolution is determined to be $18 \pm 2\mu$m. The intrinsic resolution as the function of θ is drawn in fig. 13.

7 Conclusion

We have studied the performance of a large area silicon microstrip detector of 25 μm strip pitch and 50 μm readout pitch. With the signal to noise ratio of 23, the intrinsic resolution of perpendicular track is determined to be $3.5 \pm 1\mu$m by unweighted linear fit. This is accomplished with the η correction on cluster position and linear track fitting with the multiple scattering calculated by GEANT simulation.

Study on the angular dependence by inclined tracks has shown good agreement with geometrical correlation to the cluster total charge and the cluster profile. The results seen suggest that charge collection efficiency is uniform throughout the depth of the detector. Applying the best found position-finding algorithm for various track angle, the spatial resolution of inclined tracks has been determined.

Acknowledgements

We are grateful to the Si group of ERSO for the fabrication of test samples. We thank C.Y. Chien and members of Johns Hopkins University for their support on data acquisition. We thank W. Burger for his advice and assistance on detector assembly. We also thank J.G. Ding and members of Perugia University for their assistance and encouragement. This work was supported by the National Science Council of the Republic of China under contracts NSC 82-0212-M-008-34 and NSC 83-0208-M-008-047.

References

[1] GEANT Version3.15; R.Brun *et al.*, "GEANT 3", CERN DD/EE/84-1 (Revised), September 1987.

[2] Wen-Chin Tsay *et al.*, Nucl. Instr. and Meth. A351 (1994) 463.

[3] S. Kleinfelder *et al.*, Proc. IEEE NSS Symposium, October 1989.

[4] F. Kirsten and C. Haber, Proc. IEEE NSS Symposium, October 1989.

[5] E. Belau et al., Nucl. Instr. and Meth. A214 (1983) 253.

[6] G. Lutz, Nucl. Instr. and Meth. A273 (1988) 349.

[7] R. Turchetta, Nucl. Instr. and Meth. A335 (1993) 44.

Figure Captions

Fig. 1 The test beam setup. The first setup above has been used for the study of spatial resolution; the second setup below, for the study of angular dependence.

Fig. 2 The distribution of cluster total charge fitted by a Gaussian convoluted Landau distribution. The most probably value is 28 ADC counts, corresponding to a S/N ratio of about 23.

Fig. 3 The η distribution of $N9$ detector.

Fig. 4 The $(X_\eta - X_{max})$ distribution of $N9$ detector in units of readout pitch.

Fig. 5 The rms of residuals of linear fit on the simulation of six detectors at their corresponding beam line positions. The intrinsic resolutions are simulated as Gaussian smearing of rms equals 0, 5, 7, and 10 μm to all detectors.

Fig. 6 The rms of residuals of the detector excluded in the linear fit at their corresponding beam line positions. The intrinsic resolutions are simulated as Gaussian smearing of rms equals 0, 5, 7, and 10 μm to all detectors.

Fig. 7 The residuals of $N9$ detector (data points) with a Gaussian fit (solid line). The GEANT calculation (dot line) has the intrinsic resolution simulated by $\sigma_{I.R.}$=3.5 μm.

Fig. 8 The geometry of inclined track and projections on detectors measuring horizontal and vertical coordinates.

Fig. 9 The distribution of cluster total charge at different track θ angle.

Fig. 10 The cluster total charge as the function of θ. The lines are function of $Q_0/\cos\theta$ for *horizontal* and *vertical* detectors respectively.

Fig. 11 The cluster profiles seen by the *horizontal* detector at θ angle as indicated. Distributions are the constituent strip center to the cluster position weighted by the ratio of strip signal to the cluster total charge.

Fig. 12 The width of cluster profile as the function of θ. The sagitta of W=320μm$\times\tan\theta$ is drawn as the solid line.

Fig. 13 The intrinsic resolution of *vertical* detector as the function of track θ angle.

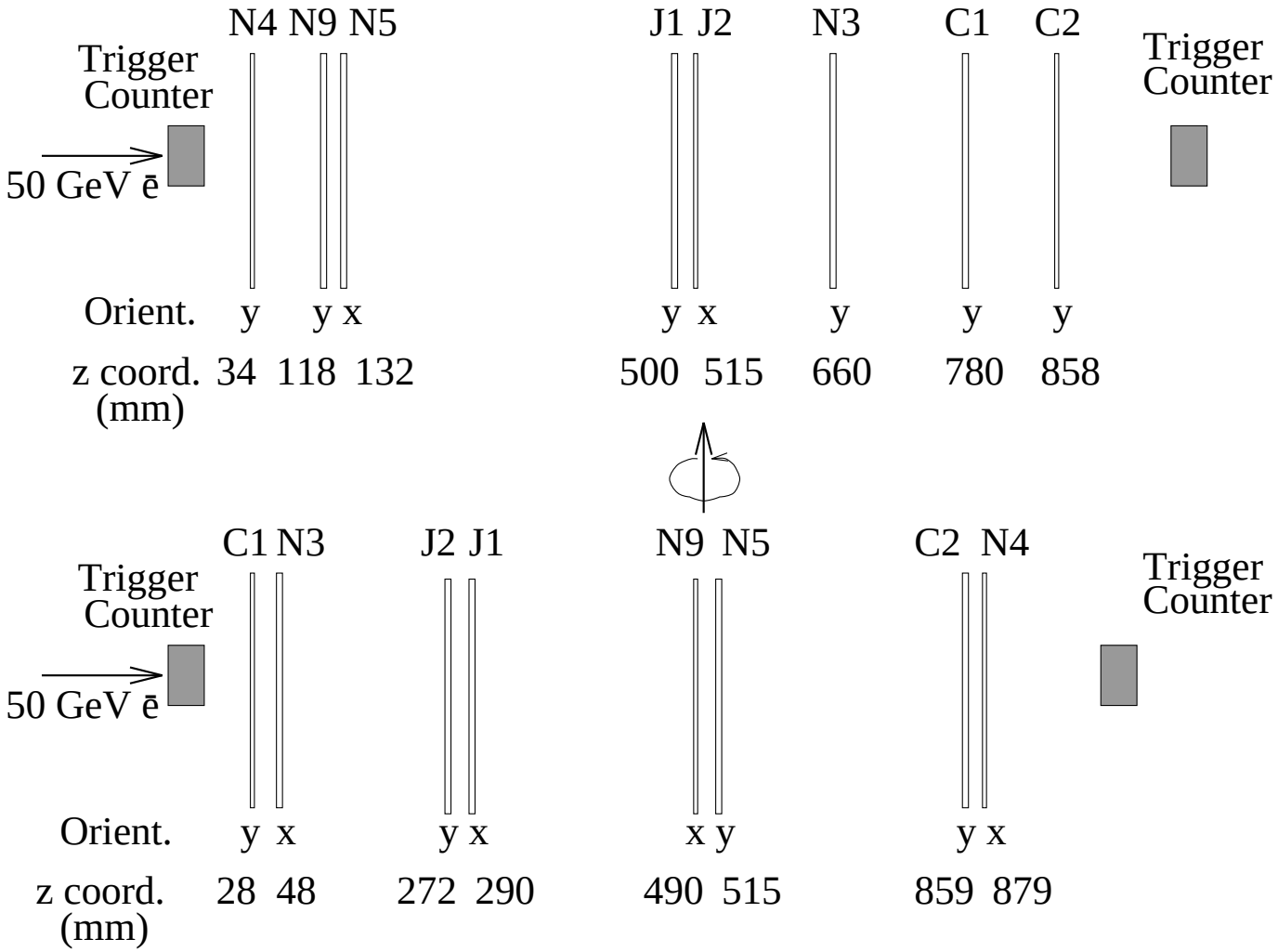
N4 N9 N5
J1 J2
N3
C1
C2
Trigger Counter
Trigger Counter
50 GeV ē
Orient.
y y x
y x
y
y
y
z coord. (mm)
34 118 132
500 515
660
780
858
C1 N3
J2 J1
N9 N5
C2 N4
Trigger Counter
Trigger Counter
50 GeV ē
Orient.
y x
y x
x y
y x
z coord. (mm)
28 48
272 290
490 515
859 879

Figure 1:

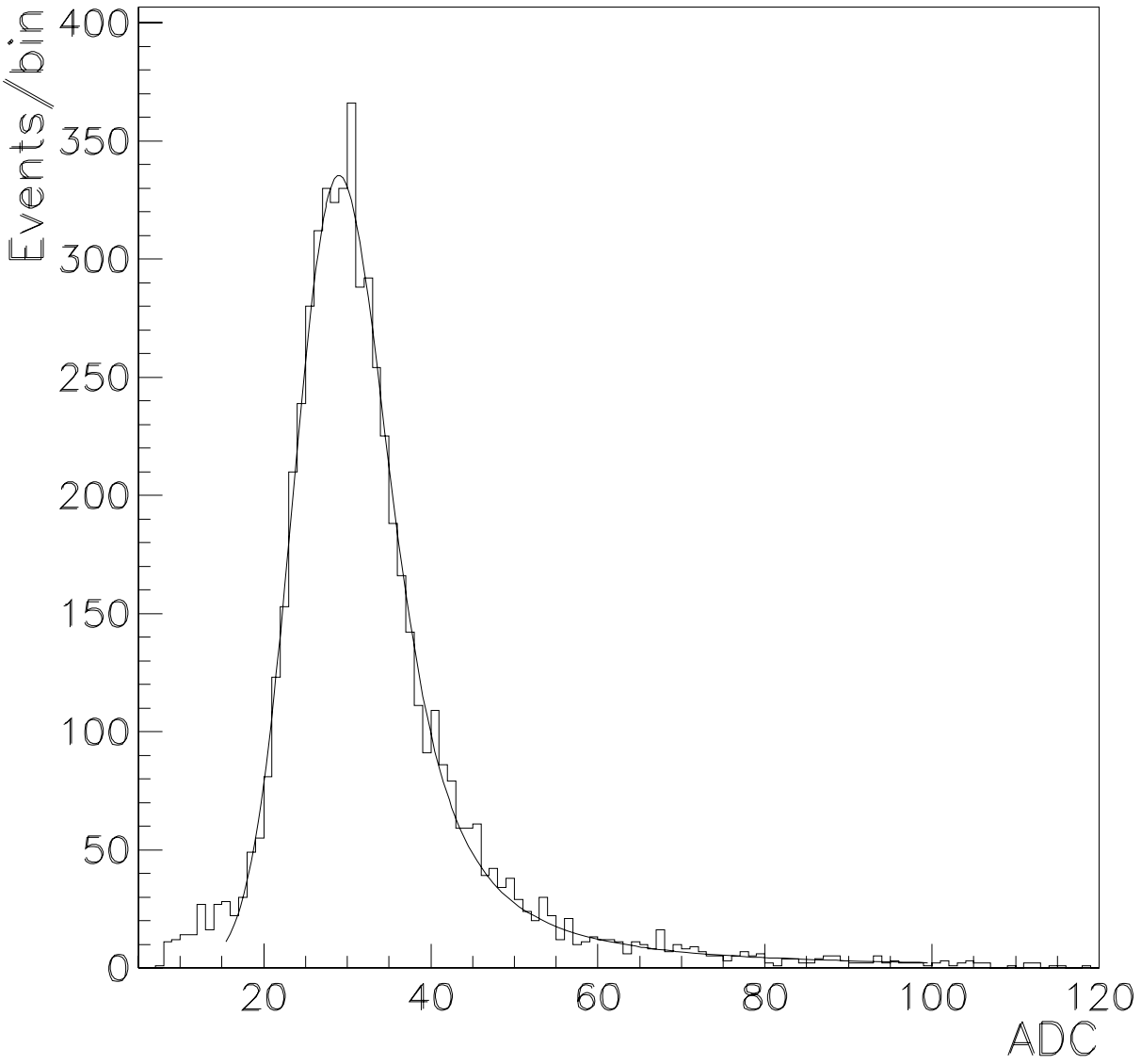
Events/bin
400
350
300
250
200
150
100
50
0
20
40
60
80
100
120
ADC

Figure 2:

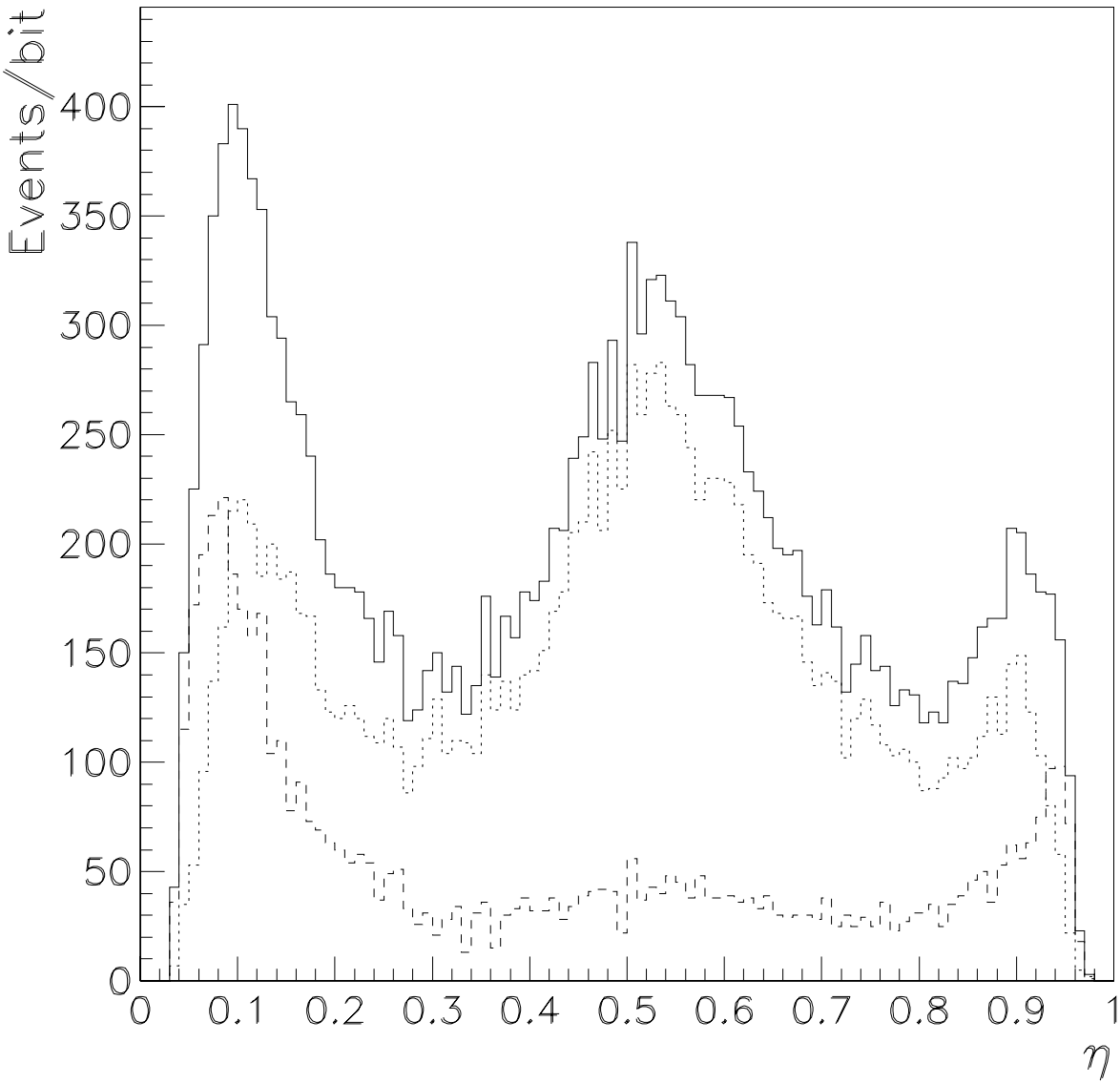
Events/bit
400
350
300
250
200
150
100
50
0
0
0.1
0.2
0.3
0.4
0.5
0.6
0.7
0.8
0.9
1
η

Figure 3:

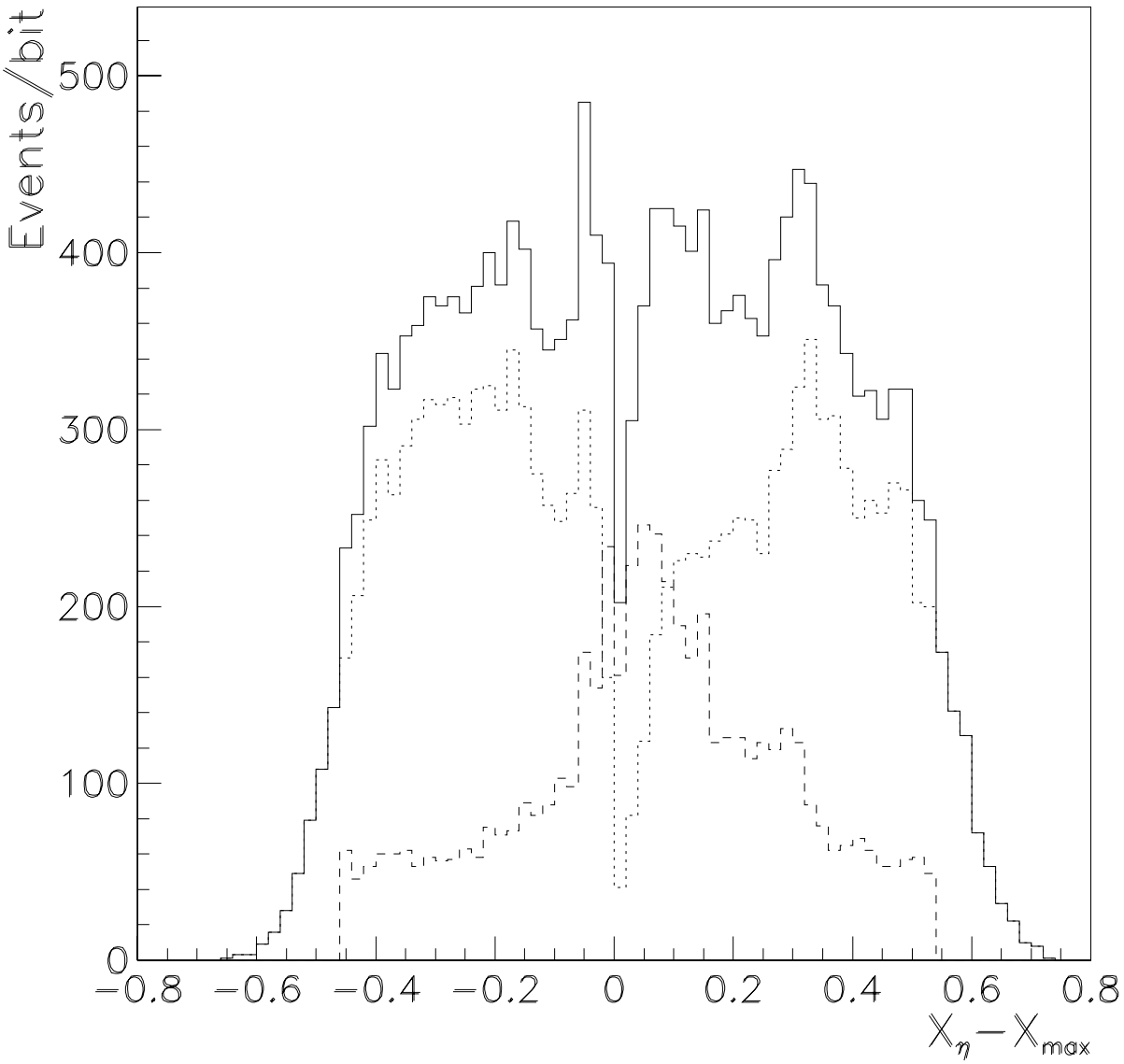
Events/bit
500
400
300
200
100
0
−0.8
−0.6
−0.4
−0.2
0
0.2
0.4
0.6
0.8
$X_\eta - X_{max}$

Figure 4:

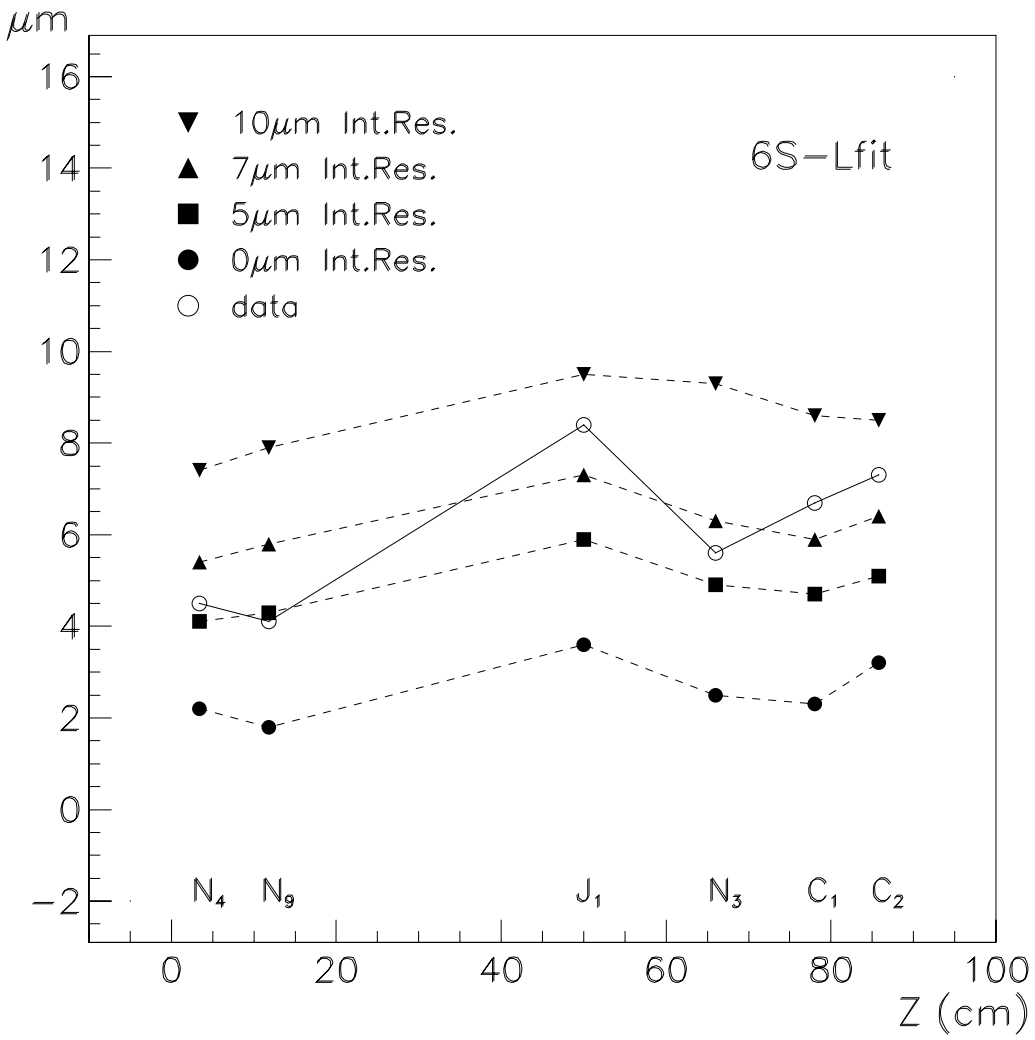
μm
16
14
12
10
8
6
4
2
0
−2
10μm Int.Res.
7μm Int.Res.
5μm Int.Res.
0μm Int.Res.
data
6S−Lfit
N4
N9
J1
N3
C1
C2
0
20
40
60
80
100
Z (cm)

Figure 5:

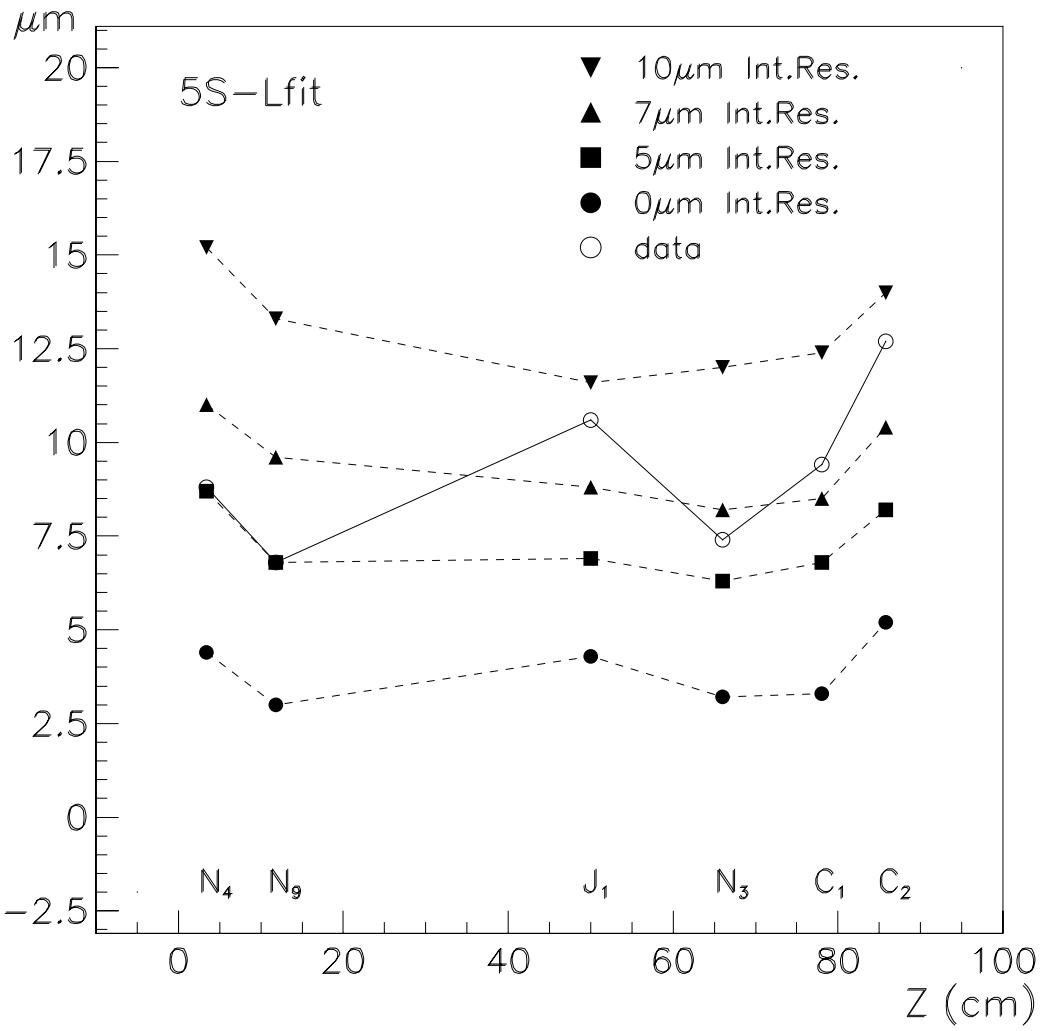
μm
20
17.5
15
12.5
10
7.5
5
2.5
0
−2.5
5S−Lfit
10μm Int.Res.
7μm Int.Res.
5μm Int.Res.
0μm Int.Res.
data
N4
N9
J1
N3
C1
C2
0
20
40
60
80
100
Z (cm)

Figure 6:

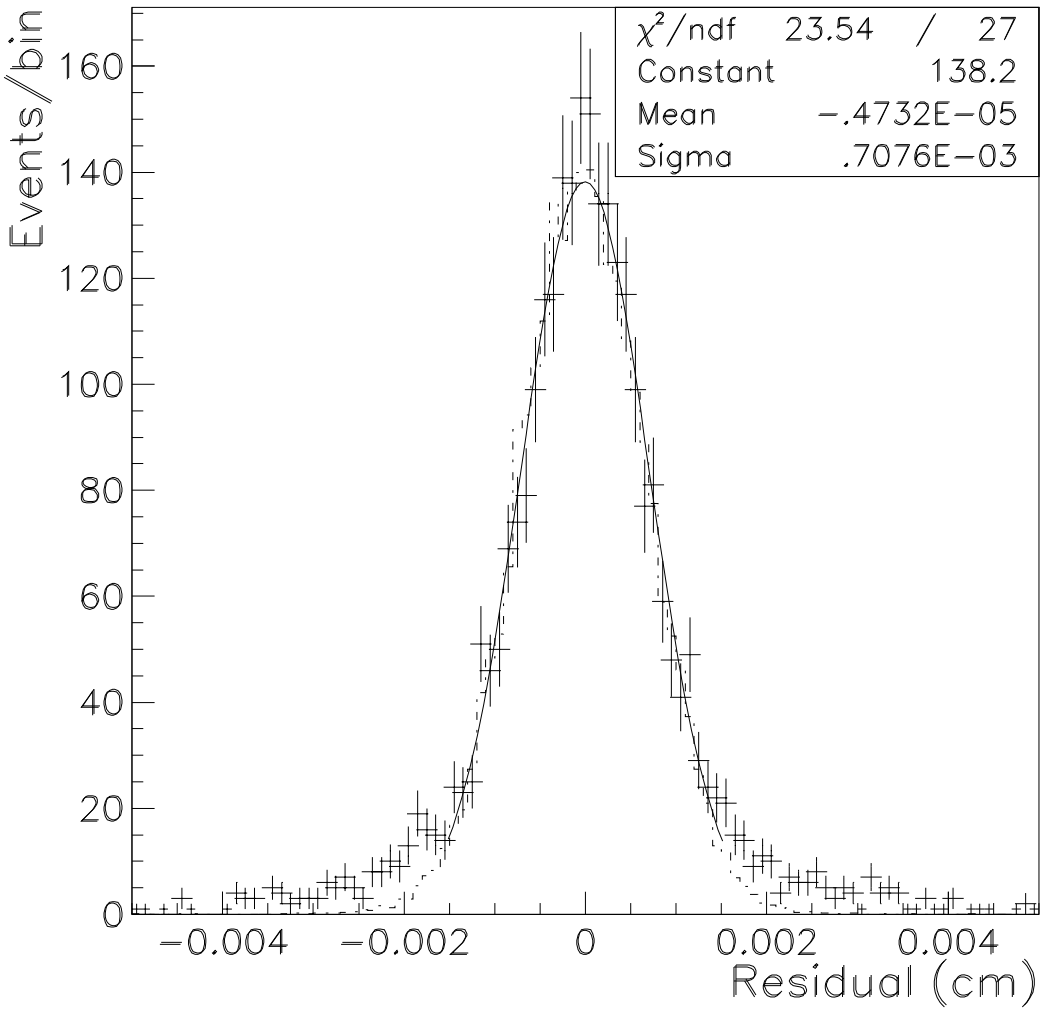
χ^2/ndf 23.54 / 27
Constant 138.2
Mean −.4732E−05
Sigma .7076E−03
Events/bin
0
20
40
60
80
100
120
140
160
−0.004
−0.002
0
0.002
0.004
Residual (cm)

Figure 7:

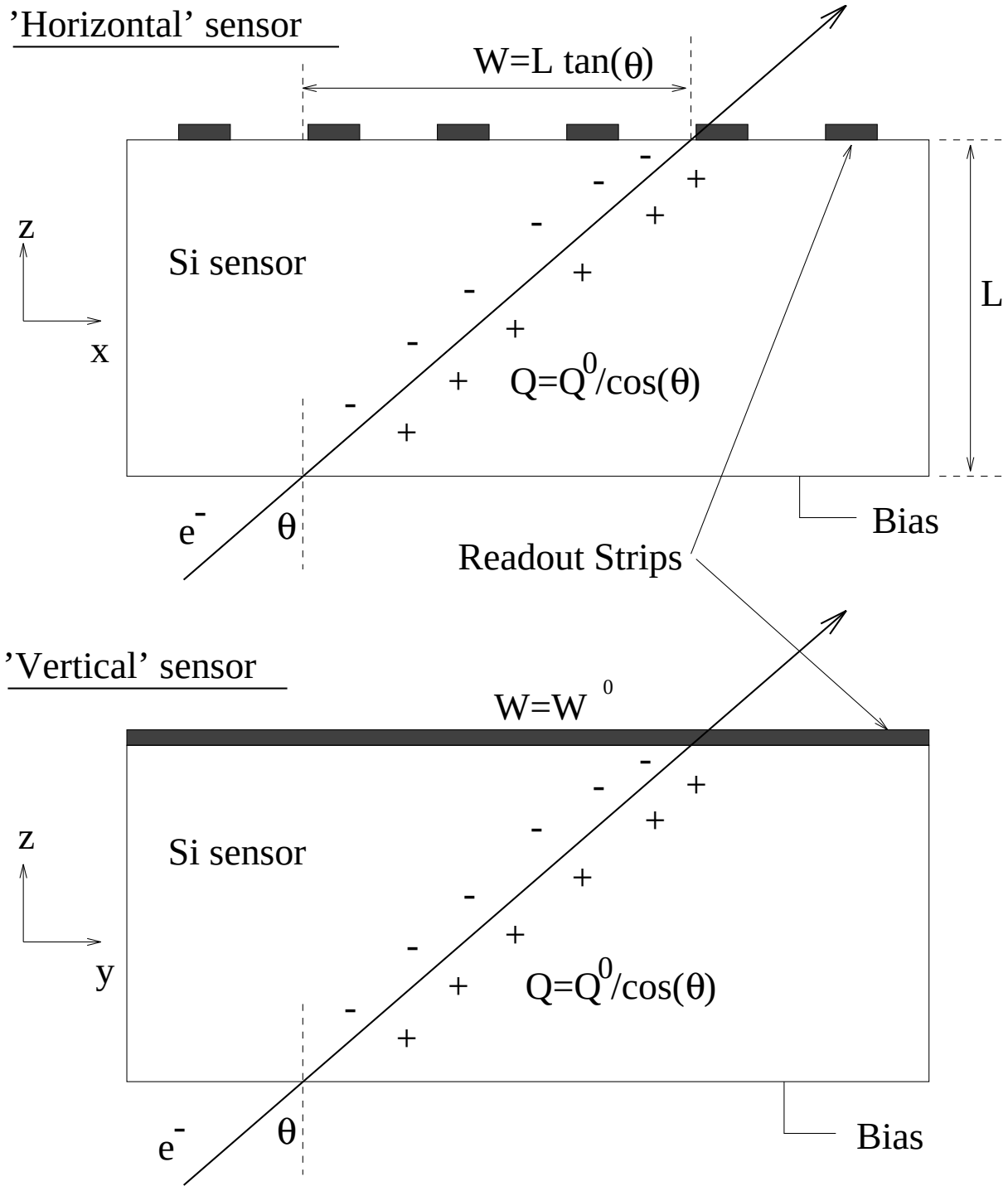
'Horizontal' sensor
W=L tan(θ)
z
x
Si sensor
L
Q=Q0/cos(θ)
e-
θ
Bias
Readout Strips
'Vertical' sensor
W=W 0
z
y
Si sensor
Q=Q0/cos(θ)
e-
θ
Bias

Figure 8:

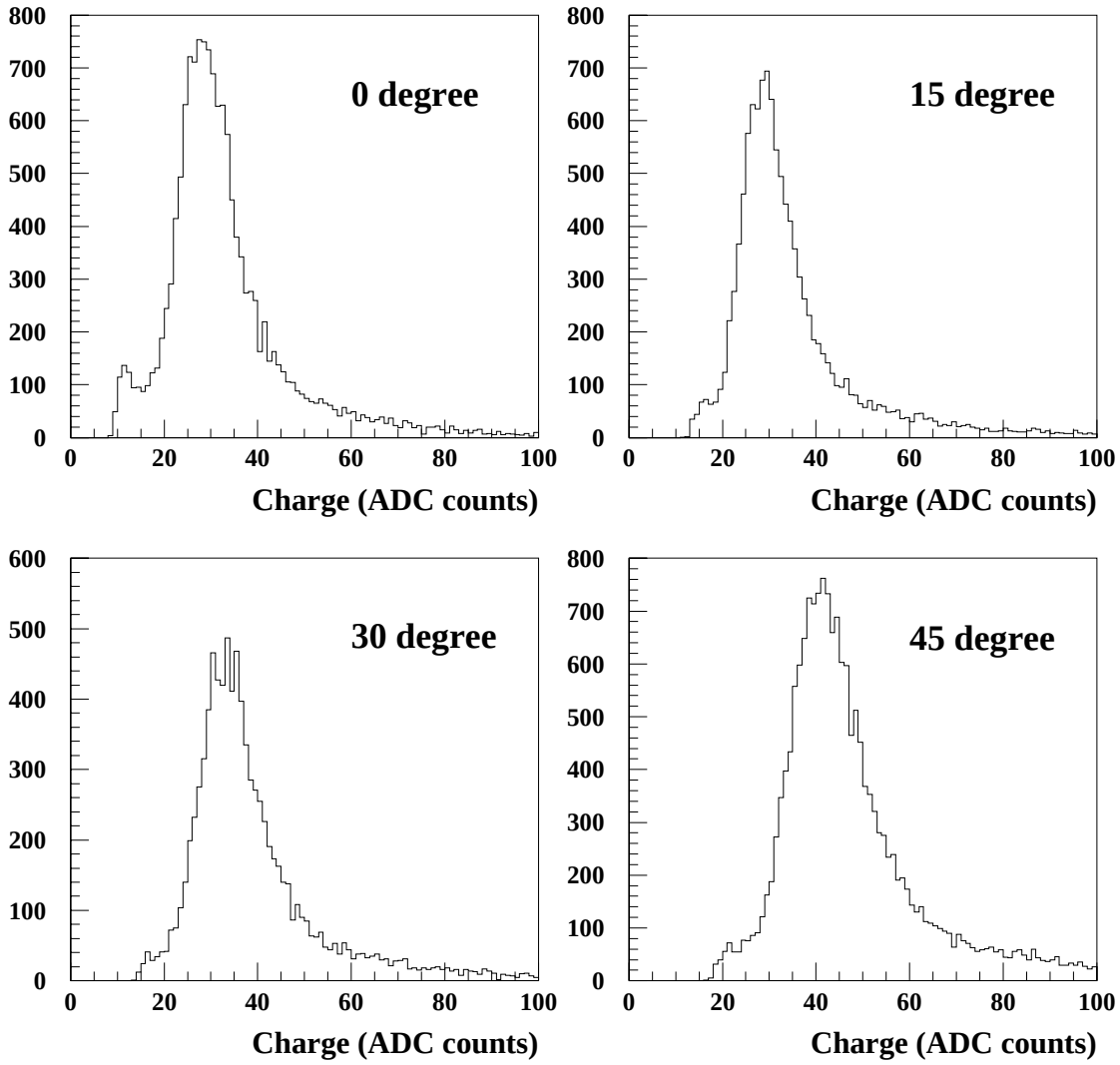
0 degree
15 degree
30 degree
45 degree
Charge (ADC counts)
Charge (ADC counts)
Charge (ADC counts)
Charge (ADC counts)

Figure 9:

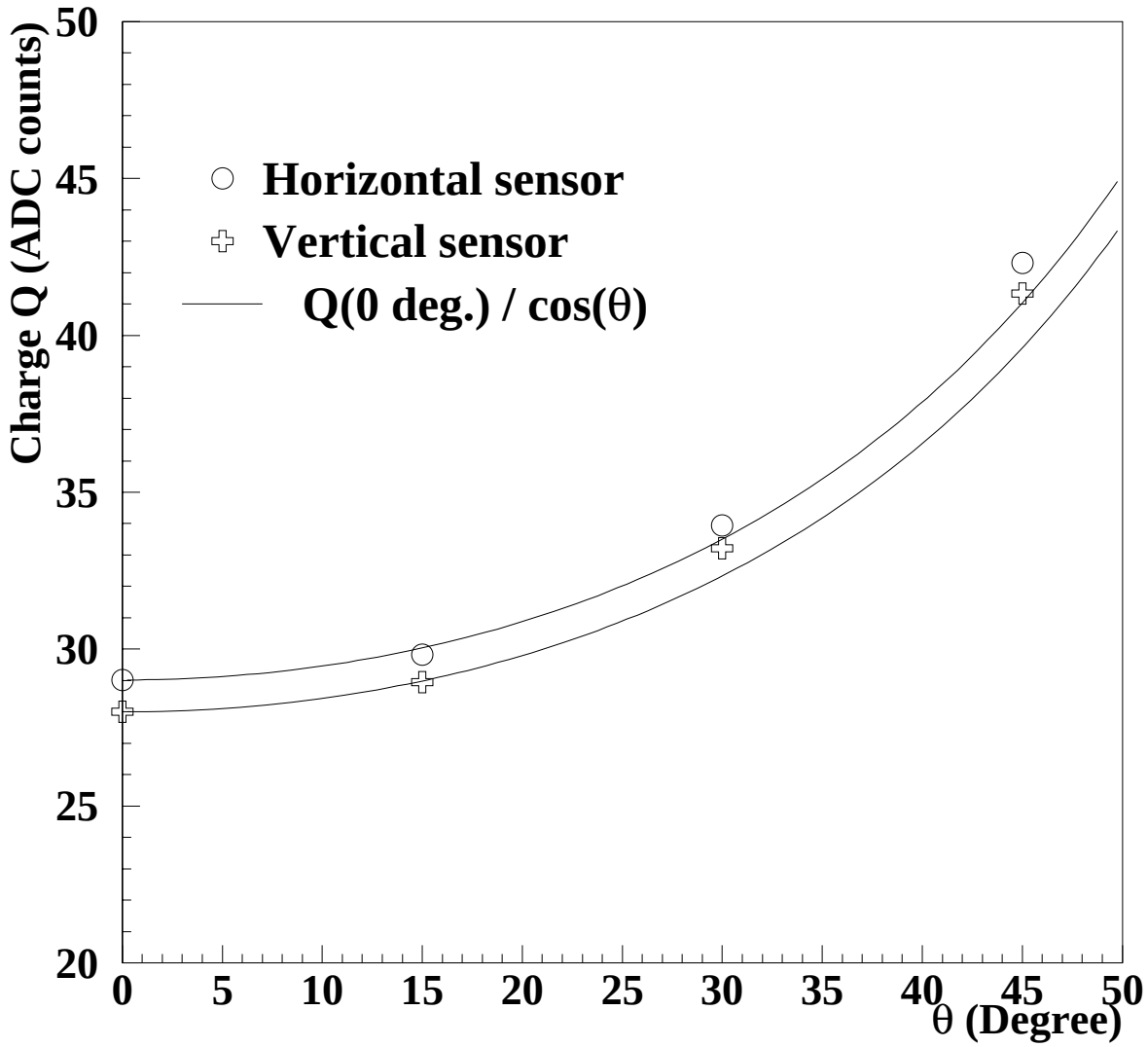
Charge Q (ADC counts)
50
45
40
35
30
25
20
Horizontal sensor
Vertical sensor
Q(0 deg.) / cos(θ)
0
5
10
15
20
25
30
35
40
45
50
θ (Degree)

Figure 10:

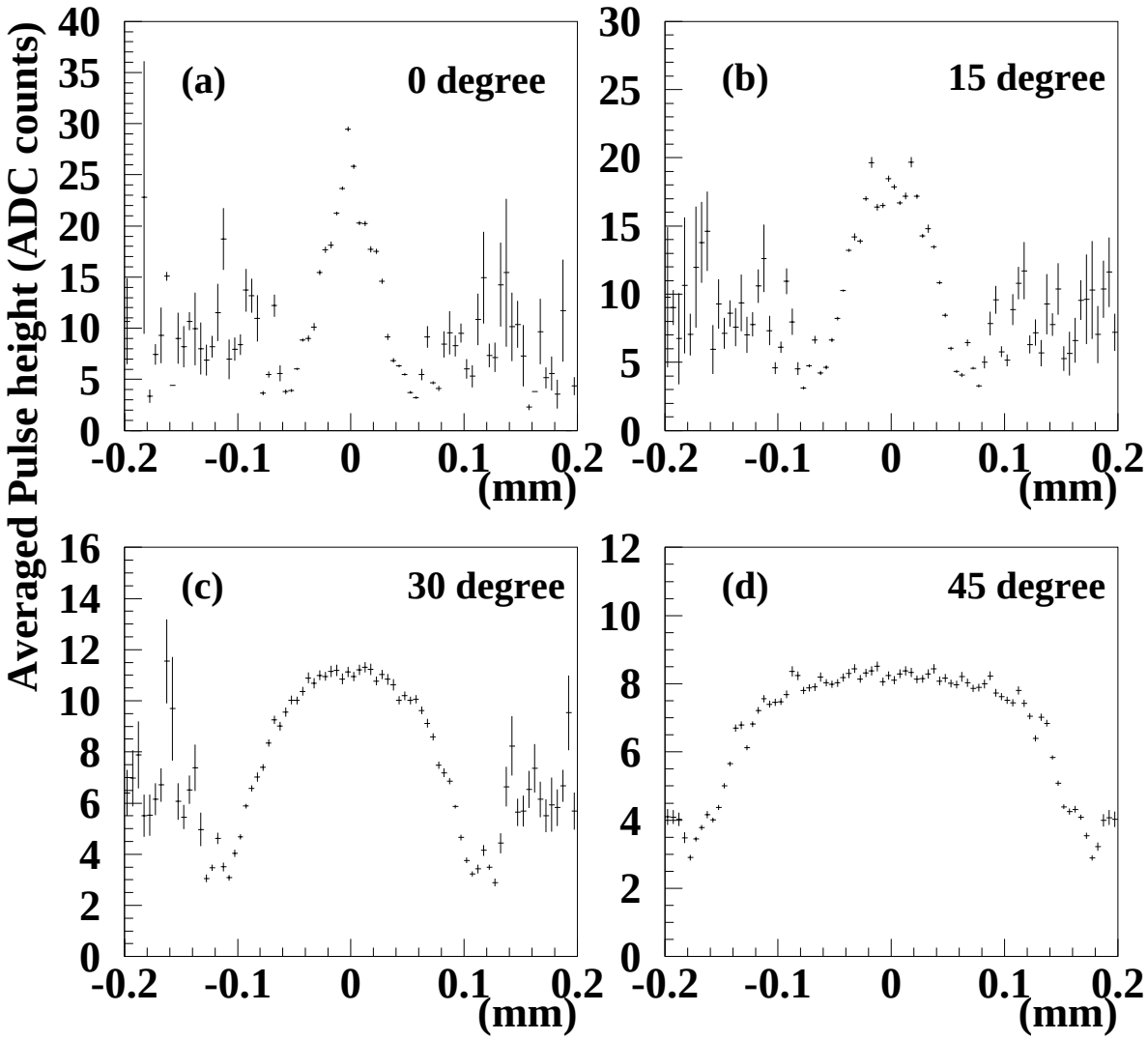
Averaged Pulse height (ADC counts)
(a)
0 degree
(b)
15 degree
(c)
30 degree
(d)
45 degree
(mm)
(mm)
(mm)
(mm)

Figure 11:

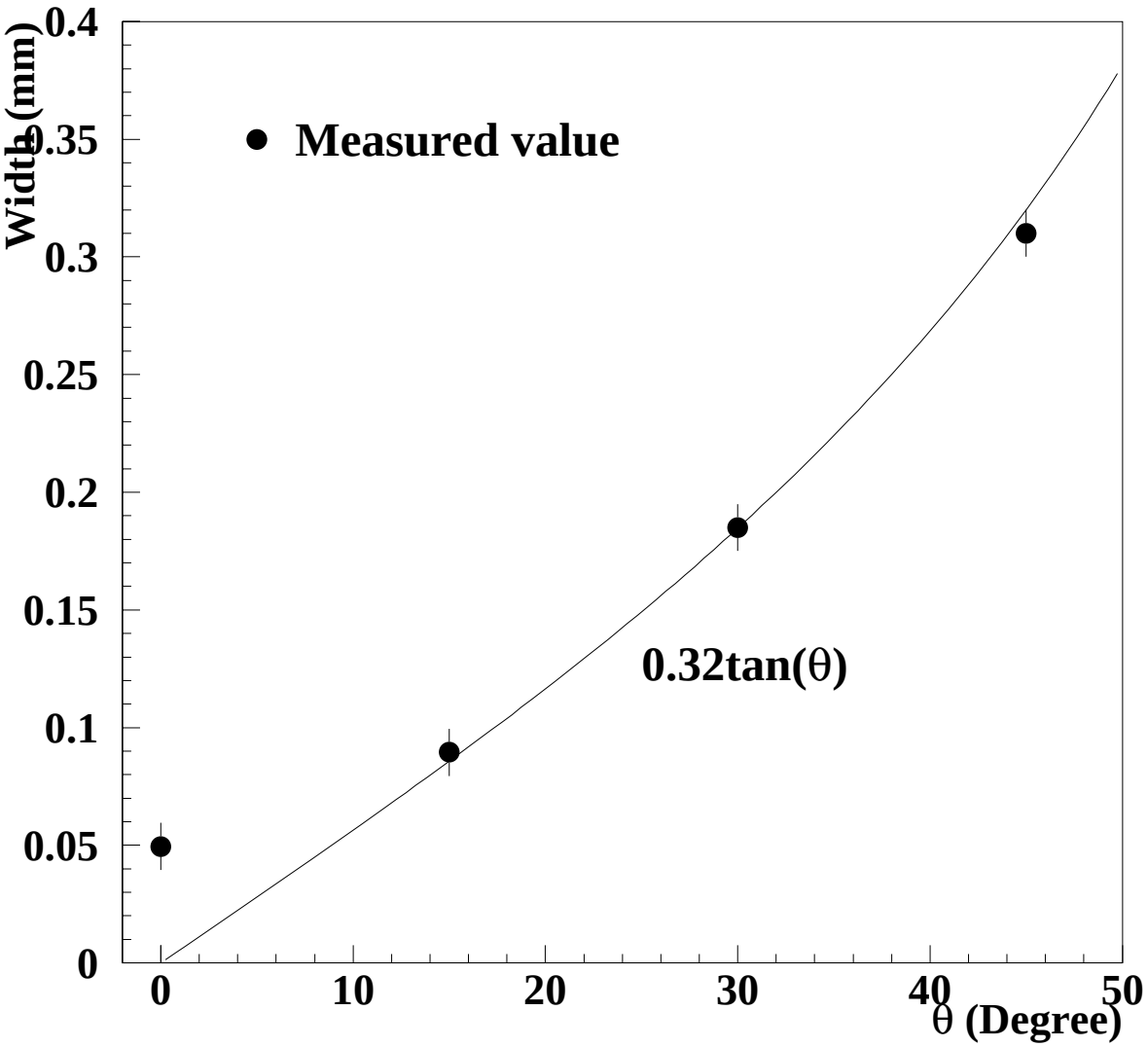
Width (mm)
0.4
0.35
0.3
0.25
0.2
0.15
0.1
0.05
0
Measured value
0.32tan(θ)
0
10
20
30
40
50
θ (Degree)

Figure 12:

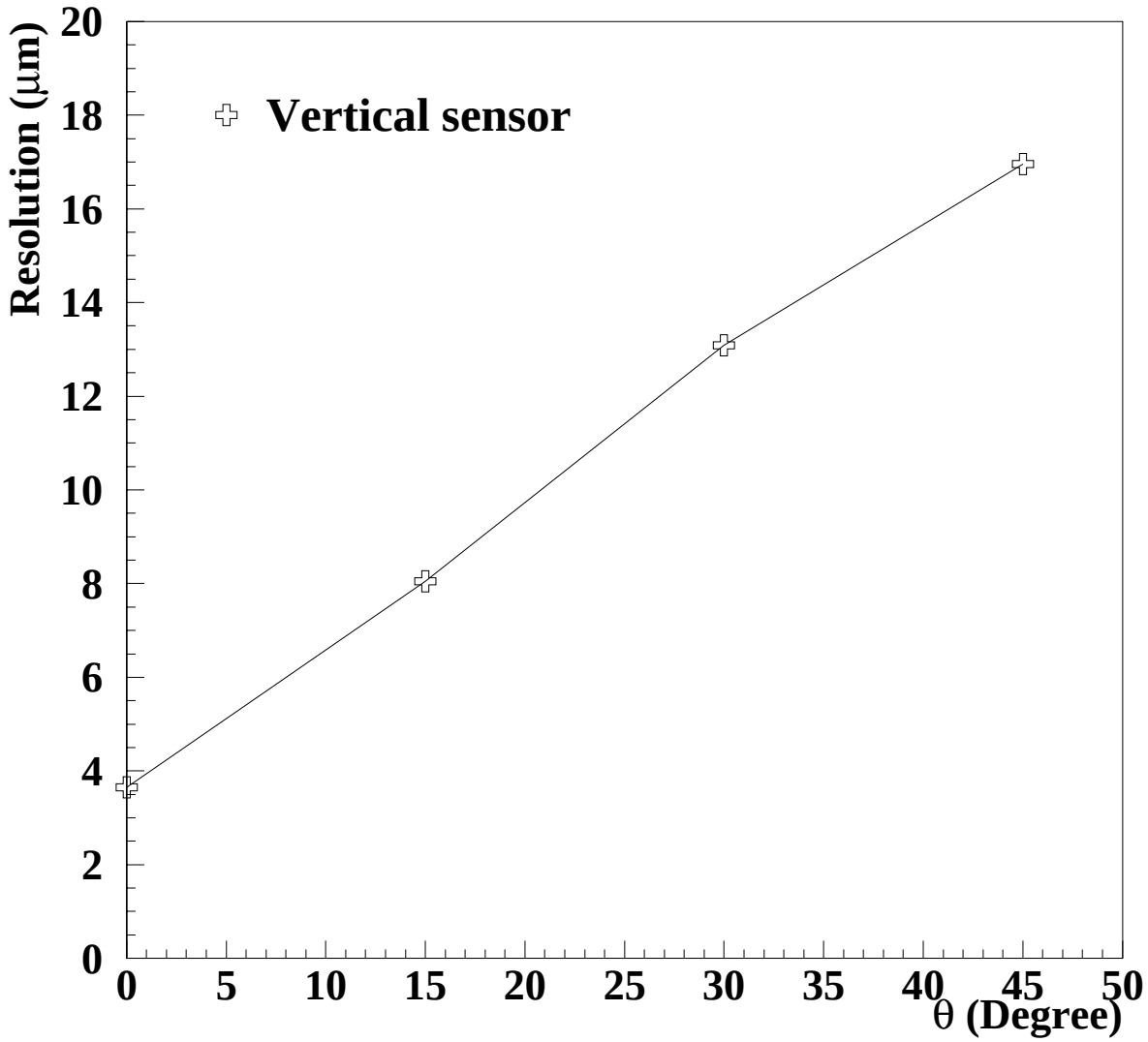
Resolution (μm)
Vertical sensor
θ (Degree)
0
2
4
6
8
10
12
14
16
18
20
0
5
10
15
20
25
30
35
40
45
50

Figure 13: